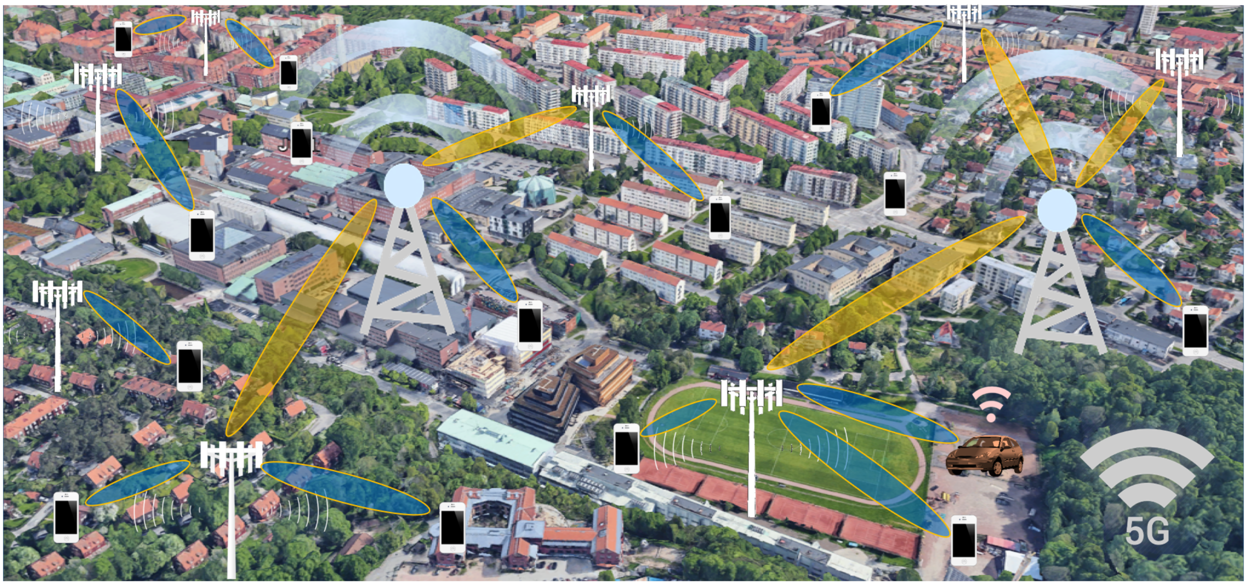

Integrated Access and Backhaul for 5G and Beyond

Master's thesis in Master Programme of Communication Engineering

CHARITHA MADAPATHA

Department of Electrical Engineering
CHALMERS UNIVERSITY OF TECHNOLOGY
Gothenburg, Sweden 2020

Master's thesis 2020:NN

Integrated Access and Backhaul for 5G and Beyond

CHARITHA MADAPATHA

Department of Electrical Engineering
Wireless Systems Division
Communication Systems Group
Chalmers University of Technology
Gothenburg, Sweden 2020

Integrated Access and Backhaul for 5G and Beyond
CHARITHA MADAPATHA

Supervisors: Behrooz Makki, Ericsson Research, Tommy Svensson, Department of Electrical Engineering, Chalmers
Examiner: Tommy Svensson, Department of Electrical Engineering, Chalmers

Master's Thesis 2020:NN
Department of Electrical Engineering
Wireless Systems Division
Communication Systems Group
Chalmers University of Technology
SE-412 96 Gothenburg
Telephone +46 31 772 1000

Cover: Integrated Access and Backhaul showing a typical use case in urban environment.

Typeset in LaTeX
Printed by Chalmers Reproservice
Gothenburg, Sweden 2020

Integrated Access and Backhaul for 5G and Beyond
CHARITHA MADAPATHA
Department of Electrical Engineering
Chalmers University of Technology

Abstract

The need to densify base station placements due to the coverage limited high frequencies is one key challenge for 5G and beyond communication systems. Fiber backhauling between these large number of base stations bring about many issues including regulatory restrictions, cost and time. Integrated access and backhauling (IAB), of which a fraction of massive available mmWave spectrum is used to backhaul is an attractive candidate solution which can support these challenges in dense 5G NR deployment.
In this thesis, we first introduce and analyze IAB as an enabler for dense networks. We study IAB networks from different perspectives including IAB use cases. As the second part, the work is performed focusing on mmWave based communications where we evaluate the performance of IAB networks in both dense and rural areas. We study the service coverage probability defined as the event that the probability of instantaneous data rates of UEs exceeds the minimum threshold rate. Here, the IAB nodes and user equipments (UEs) are distributed in a finite region using a stochastic geometry model.
We present cost-performance comparisons between the IAB networks and the cases where all or part of the small BSs are fiber-connected. Then, we study the effect of blockage, tree foliage, as well as the rain on the service coverage probability of IAB networks. Following the stochastic model based system analysis, we use OpenStreetMap data and locate the BSs on top of geo data and observe the network performance in the presence of realistic terrain and building information.
Finally we compare the IAB network with a traditional fiber backhauled network and a hybrid network where some selected small base stations are fiber connected while the others are IAB nodes. Following the analysis, it is observed that IAB remains a better solution for the key challenges in the network including cost while maintaining the needed performance levels.

Keywords: Integrated access and backhaul, IAB, millimeter wave (mmWave) communications, 3GPP, Stochastic geometry, Poisson point process, Coverage probability, Germ-grain model, ITU-R, FITU-R, Wireless backhaul, 5G NR

Acknowledgements

Firstly, my heartfelt gratitude goes to Professor Tommy Svensson, for giving the nicest opportunity to conduct this thesis and also for guiding me throughout the period including the summer internship. His valuable research ideas not only supported me to conduct the techincality of the project in good shape, but also helped to have much important lessons worth for my future both in academics as well as keeping the balance in life practices. The regular friendly meetings even in tight schedules, and the motivation you brought at those were immense. When there was some issue to be discussed you were always there.

I would like to thank Dr. Behrooz Makki, for always been there to support and guide the work which finally came this end. He was always enthusiastic on this project and was communicating throughout with advisories regarding the technicalities and general practices. Also a broader industrial support and insights were brought in thanks to his experiences and contacts at Ericsson. My heartiest gratitude goes towards the motivation and knowledge you brought in.

Then my thanks goes to Chao Fang who was always there during the meetings to commend and suggest the way forward. Ericsson and its IAB researchers including Mikeal Coldrey are thanked for the valuable comments and knowledge they provided.

Furthermore I would like to thank the electrical engineering department of Chalmers University of Technology and its team for providing the much needed infrastructure and facilities.

Also it is very unfair, if I forget to acknowledge the Swedish Institute which provided me the most valuable scholarship to fund me all throughout the stay during my master's. Things would have been very different if such support was not granted.

Finally I would like to thank my parents and the beloved ones, for always been there to give me the much needed hand and love on whatever the ups and downs I had through the life journey.

All your support and this valuable time will be heartily remembered throughout. "Gratitude is when memory is stored in the heart and not in the mind." – Lionel Hampton

Charitha Madapatha, Gothenburg, May 2020

List of acronyms

BS	Base Stations
CI	Close-in
FDD	Frequency Division Duplex
FHPPP	Finite homogeneous Poisson point process
FITU-R	Fitted International Telecommunication Union-Radio communication sector
GSM	Global System for Mobile
HetNet	Heterogeneous Network
HPPP	Homogeneous Poisson Point Process
IAB	Integrated access and backhaul
ITU-R	International Telecommunication Union-Radio communication sector
LOS	Line-of-sight
LTE	Long Term Evolution
MBSs	Macro Base Station
MIMO	Multiple-Input-Multiple-Output
mmWave	millimeter wave
NLOS	Non line-of-sight
PPP	Poisson Point Processes
QoS	Quality of service
SBSs	Small Base Station
SINR	Signal-to-Interference-plus-Noise Ratio
TDD	Time Division Duplex
UAV	Unmanned Aerial Vehicle
UE	User Equipment
UMa	Urban Macro
UMTS	The Universal Mobile Telecommunications System
3GPP	3rd Generation Partnership Project
5G NR	5G New Radio

Contents

List of Figures

List of Tables

1

Introduction

Network densification is a main driving force in the route to 5G and beyond deployments due to the coverage limited high frequencies. This is an integral component in providing massively increased data throughputs and has become a feasible scenario due to the introduction of low power SBS technologies. However, one of the main obvious hindrance is the cost involved when connecting these massive number of SBSs in to fiber network for backhauling. Thus due to the deployment constraints it is not feasible to connect all SBSs with the existing high speed fiber. Different reports, e.g, [1], predict a steep increase of Internet devices connected through wireless access as well as a massive increase in mobile traffic. Thus to cope with such requirements, the aforementioned network densification in the fifth generation (5G) wireless networks is achieved via the deployment of many base stations (BSs) of different types, so that there are more resource blocks per unit area.

Different wired and wireless technologies have been developed to support the backhauling in the network, e.g. [2]. Traditionally, wired backhauls have been deployed in urban and suburban areas with high data traffic, while wireless backhauls (including satellite [3], microwave radio [4], [5] or free space optical [6] links) has been used in places where deploying wired connections is costly. In fact, fiber optic provides high data rates supporting several Gbps for long haul [7]. However, the significant capex cost involved when deploying fiber optic is a hindrance. Also, most of these costs are for trenching and digging which in turns increase the installation times in addition to the cost. In some cases, the trenching may also not be granted permissions, e.g., metropolitan areas.

In ultra dense networks with many BSs, wireless backhauling is a very feasible option when compared with the other backhaul alternatives. Due to this, millimeter wave (mmWave)-based wireless backhauling is considered as an attractive replacement for fiber optic, which provides similar data rates with lower cost and simpler deployment effort. On this basis, integrated access and backhaul (IAB) networks, where part of the radio resources can be utilized for backhauling in a more integrated manner has gained significant attention both in industry and academia [8], [9]. The main purpose of IAB is to replace the existing costly backhaul technologies with a more flexible wireless bachkhaul using the same existing spectrum. In addition to backhaul, this brings the flexibility to provide normal cellular services within the same node. The Figure. 1.1 illustrates the use case of 5G expansion for dense networks using IAB.

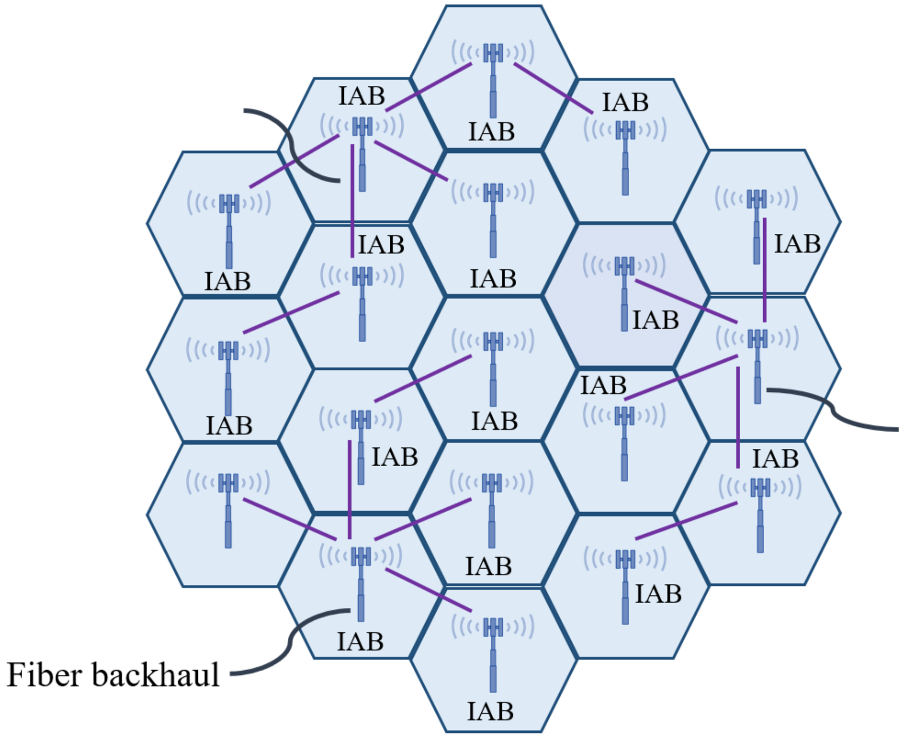

Figure 1.1: Expansion of 5G NR coverage with IAB.

Although IAB-type relayed backhaul has been studied for LTE networks previously, the commercial deployments were limited mainly due to the expensive spectrum in sub-6 GHz band [10].
However, in 5G new radio (NR) IAB is expected be more successful due to the massive bandwidth available in mmWave spectrum. Also, the fact that mmWave access having short propagation range also increases the demand for densified deployments where IAB can act as an enabler. Moreover, NR inherits highly directional beamforming capabilities and multiple-input-multiple-output (MIMO), which helps to mitigate the cross-link interference between access and backhaul liks. Currently, IAB is being standardized for 3GPP Rel-16 [11], and the process will continue in Rel-17.
IAB is a relatively new research area, and thus has been studied in few works only. In [12]-[15], cost-optimum node placement and resource allocation is studied while [12]-[17] studied routing in the multi hop cases. Moreover, [18], studies the extended coverage area using multi hop relaying while [19] perform end-to-end feasibility check on mmWave IAB networks through simulations. Also, [20, 21] verifies and evaluated the effect of dynamic time division duplex (TDD)-based resource allocation on the throughput metrics of IAB networks. Also, [22]-[24] studies the behaviour of coverage probability in IAB networks using Poisson point processes (PPPs). Finally, [25], and [26] investigates on the power allocation to maximize the sum rate and on the usefulness of IAB in unmanned aerial vehicle (UAV)-based communications respectively.
We study the performance of IAB networks from different perspectives. Focusing on

a mmWave-based communication system we analyze the service coverage probability defined as the ratio of the UEs whose minimum rate requirements are satisfied, and then we compare them with a fully fiber-connected and partially fiber-connected hybrid IAB network. Here, the results are presented for the cases with a finite homogeneous Poisson point process (FHPPP)-based stochastic geometry model where IAB nodes and UEs are randomly distributed in a finite region. Later we deploy the network in OpenStreetMap terrain and topography profile to evaluate the performance in 3D space in terms of antenna heights.
One contrasting difference between IAB and fiber-connected networks is that, unlike the fiber links IAB channels are prone to affected by the environmental effects such the rain, the blockage as well as the tree foliage. Thus, we evaluate the effect of the rain, the blockage, the BSs heights, the antenna array gains as well as the tree foliage on the robustness of IAB networks. Here, the results are presented for both rural and urban areas, while we mainly concentrate on dense networks, as the most interesting use case in IAB.

2

System Model

We consider an outdoor two tier heterogeneous network (HetNet) with multiple MBSs (M: macro), SBSs (S: small) and UEs are distributed as shown in Figure. 2.1. The MBSs and SBSs are generally referred as the donors and child IABs of the system. In an IAB deployment, both the MBSs and the SBSs use wireless channels for both access and backhaul in a more integrated manner. Moreover, at the beginning only the MBSs are fiber-connected while the SBSs receive data from the MBSs. The available bandwidth is dynamically shared among access and backhaul links of the IAB nodes such that the network service coverage probability is maximized. In our analysis, the MBSs and SBSs are having constant power over the spectrum and are active.

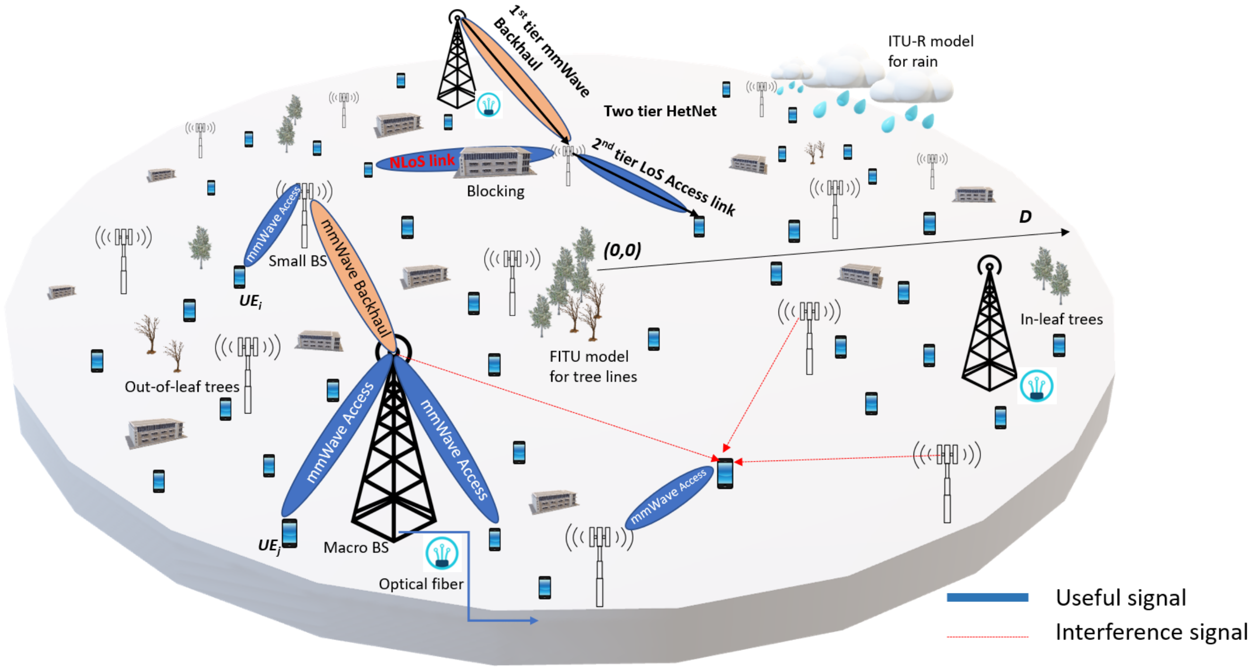

Figure 2.1: Schematic of system model.

Table 2.1: The definition of the parameters.

Parameter	Definition	Parameter	Definition
ϕ_{M}	FHPPP of MBSs	ϕ_{U}	FHPPP of UEs
ϕ_{S}	FHPPP of SBSs	λ_{U}	UE density
ϕ_{B}	FHPPP of blocking walls	θ	Orientation of blocking wall
ϕ_{T}	FHPPP of tree lines	l_{hop}	Average hop length
λ_{M}	MBS density	λ_{S}	SBS density
λ_{S}	SBS density	H	Homogeneous Poisson Process
λ_{B}	Blocking wall density	x_0	Center point of circular disk
A	Circular disk	D	Radius of the disk
P_{t}	Transmission power	P_{r}	Received power
h	Fading power	G	Antenna gain
w	SBSs antenna height	$L_{(1\mathrm{m})}$	Reference path loss at 1 meter distance
L	Propagation path loss	x	Location of the node
r	Propagation distance between the nodes	α	Path loss exponent
f_{c}	Carrier frequency	l_{B}	Blocking wall length
φ	Angle between the BS and UE	θ_{HPBW}	Half power beamwidth of the antenna
G_0	Maximum gain of directional antenna	$g(\varphi)$	Side lobe gain
R_{th}	Minimum data rate threshold	x_{c}	Associated cell
R	Rain intensity	F_{T}	Tree foliage
γ_{R}	Rainloss	d	Vegetation depth
B	Bandwidth of the DL	μ	Percentage of bandwidth resources on backhaul
l_{T}	Tree line length	λ_{T}	Tree blocking density

2.1 Spatial Model

Table 2.1 summarizes the definitions of the parameters used in the analysis. We model the IAB network using a FHPPP, [26]. Furthermore, FHPPPs ϕ_{M} and ϕ_{S} with densities λ_{M} and λ_{S}, respectively, model the spatial distributions of the MBSs and the SBSs, respectively.

The FHPPP of MBSs is represented by $\phi_{\mathrm{M}} = H \cap A$, where H is a homogeneous poisson point process (HPPP) with λ_{M} density and $A \subset \mathbb{R}^2$ is a finite region. To simplify the system, without loss of generality, we use a circular disk A with radius D. Thus $A = a(x_0, D)$ where $a(x_0, D)$ represents the planar circular disk centered at x_0. Still, the study is generic and can be used on any arbitrary region A [27].

The SBSs and the UEs are also located within the previously described A complying with the two other mutually independent FHPPPs ϕ_{S} and ϕ_{U} with densities λ_{S} and λ_{U}, respectively.

2.1.1 2D Plane

We study the system performance using two blocking models. First, we use germ grain model [30, Chapter 14], which is a FHPPP, i.e., ϕ_{B} distributed in the same finite region A with density λ_{B}. The model fits well in approximating the blind spot probability for large obstacles as it considers the blocking correlation also in to account. Also this is a 2D model where, the blockings are walls with constant length and orientation θ. The walls are spatially distributed in random locations uniformly according to the FHPPP.

2.1.2 3D Plane

The 2D model does not consider the the elevation of the blocking and the BSs. Also, the terrain information of the land are not considered. Due to this, in the second model, we distribute the same FHPPP arrangement of the MBSs, the SBSs and the UEs with their heights on top of geographic map data with real blocking terrain using OpenStreetMap 3D environment. Among other scenarios, this also enables us to evaluate the effect of the antennas and blocking height on the service coverage probability (see Chapter 3.3 and Figure. 3.13).

2.2 Channel Model

We consider an in-band communication system, where both the access and backhaul links operate in the same mmWave spectrum. Following the state-of-the-art mmWave channel model, [27], the received power at each node in the network is given by

$$P_{\mathrm{r}} = P_{\mathrm{t}} h_{\mathrm{t,r}} G_{\mathrm{t,r}} T_{\mathrm{t}} L_{(1\mathrm{m})} L_{\mathrm{t,r}} \left|\left|x_{\mathrm{t}} - x_{\mathrm{r}}\right|\right|^{-1} F_{\mathrm{t,r}} \gamma_{\mathrm{t,r}}. \tag{2.1}$$

Here, P_{t} is the transmit power in the considered link, and $h_{t,r}$ denotes the independent small-scale fading. In our analysis, the fading is modelled as a normalized Rayleigh random variable [28], [29]. The $G_{t,r}$ denotes the combined antenna gain of the transmitter and the receiver of the considered link, $L_{t,r}$ is the propagation path loss, and $L_{(1m)}$ represents the path loss at reference 1 meter distance. Moreover, T_t represents the bias factor of the transmitter used to offload users while $F_{\mathrm{t,r}}$, $\gamma_{\mathrm{t,r}}$ entail the tree foliage loss and rain loss between transmitter and receiver of the link in linear scale. The total path loss, in dB scale is characterized using the 5GCM UMa close-in (CI) model in [31]. The path loss is expressed as

$$\mathrm{PL} = 32.4 + 10\log_{10}(r)^{\alpha} + 20\log_{10}(f_{\mathrm{c}}). \tag{2.2}$$

Here, f_c represents the carrier frequency, r is the distance between the nodes, and α denotes the propagation path loss exponent. Depending on the blockage, the line-of-sight (LOS) and non line-of-sight (NLOS) links have different affects. The different path loss exponents characterize this behavior. The propagation loss obtained from the path loss model is obtained as

$$L_{\mathrm{t,r}} = \begin{cases} r^{\alpha_{\mathrm{L}}}, & \text{if LoS,} \\ r^{\alpha_{\mathrm{N}}}, & \text{if NLoS.} \end{cases} \tag{2.3}$$

We model the beam patterns as a sectored-pattern antenna array and hence, the antenna gain between two respective transmitter-receiver nodes can be given by

$$G_{i,j} = \begin{cases} G_0 & \frac{-\theta_{\mathrm{HPBW}}}{2} \leq \varphi \leq \frac{\theta_{\mathrm{HPBW}}}{2} \\ g(\varphi) & \text{otherwise.} \end{cases} \tag{2.4}$$

Here, i, j represent the index of the concerned nodes and φ is the angle between the BS and UE in the considered link. Moreover, θ_{HPBW} is the half power beam-width of the antenna and G_0 is the antenna's maximum gain while $g(\varphi)$ is the side lobe gain which is far lesser in value than the main lobe. For information on how the antenna gain gets affected by the properties of antenna arrays, see [27].
We assume that the backhaul antennas have large capacity and, thus, are capable of perfect beamforming. Subsequently, we ignore the interference in the backhaul links and thus are noise limited. Additionally, the inter-UE interferences are neglected due to the low power of the UEs and with the assumption of sufficient isolation between them. On the other hand, as illustrated in Figure. 2.2, we focus on the aggregated interference on the access links, due to the neighbouring interferers, which for UE u is obtained by

$$I_u = \sum_{i,j \in \phi_{i,j} \setminus \{\mathbf{x}_c\}} P_j h_{i,j} G_{i,j} L_{(1\mathrm{m})} L_{x_i,x_j} \|\mathbf{x}_i - \mathbf{x}_j\|^{-1}. \tag{2.5}$$

Here, i and j denote any BS except the associated cell x_{c} which can either be an MBS or an SBS (See Chapter 2.4 for more information). Figure. 2.2. depicts the interference modelling used.

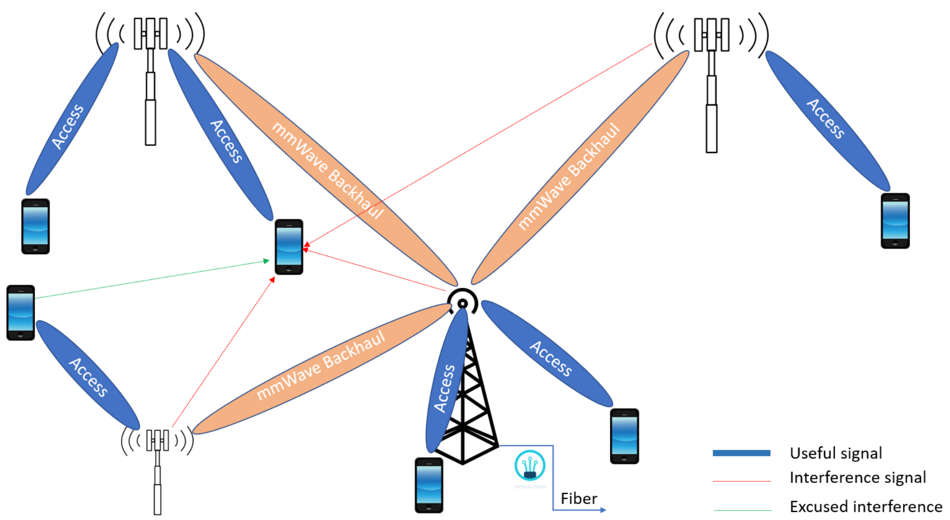

Figure 2.2: Illustration of interference model.

2.3 Effect of Rain and Tree Foliage

With the intention of understanding the performance of IAB network in rainy conditions, we use the ITU-R Rec 8.38-3 rain model [32] to introduce rain effect on the links. This is a useful model used to methodically estimate the amount of rain attenuation on different radio links. The model gives the rain loss as

$$\gamma_{\mathrm{R}} = kR^{\beta}. \tag{2.6}$$

Here, γ_{R} is the rain loss in dB/km, R is the rain intensity in mm/hr. Also, k and β denote coefficients that are precalculated depending on the carrier frequency. Table 2.2 shows the coefficients for horizontal and vertical losses at rainy conditions in 28 GHz on which we concentrate in the simulations.

Table 2.2: Coefficients for ITU-R model β_h, k_h = horizontal polarization coefficients and β_v, k_v = vertical polarization coefficients [32]

Frequency (GHz)	β_h	β_v	k_h	k_v
28	0.9679	0.9277	0.2051	0.1964

Then, FHPPP ϕ_{T} with density λ_{T} is used to model the spatial distribution of the tree lines of length l_{T} [33]. We use the Fitted International Telecommunication Union-Radio (FITU-R) tree foliage model [34, Chapter 7] to entail the effect of the trees on the links. This is a well known model for the cases with frequency dependency and non-uniform vegetation. The model can estimate tree foliage in the frequency range of 10-40 GHz. In this way, considering two states depending on the leaf availability in the tree lines, namely, in-leaf and out-of-leaf, the tree foliage in dB is obtained as

$$F_{\mathrm{T}} = \begin{cases} 0.39 f_{\mathrm{c}}^{0.39} d^{0.25}, & \text{in-leaf} \\ 0.37 f_{\mathrm{c}}^{0.18} d^{0.59}, & \text{out-of-leaf.} \end{cases} \tag{2.7}$$

Here, f_{c} represents the carrier frequency expressed in MHz and d is the vegetation depth in m. The tree foliage loss is higher in the in-leaf conditions than the out-of leaf conditions. The model is applicable for regions with different seasons that has varying tree leaf content depending on the time of the year. Moreover, the estimated tree foliage through this model is very much relying on the nature of the vegetation and the amount of leaf content found.

2.4 Association and Allocation Strategy

In our setup, the user can be served by either an MBS or an SBS based on maximum average received power rule following an open access strategy. In this way, the association rule for UE u suffices

$$\sum_{\forall j} u_j = 1,\ \forall_u \in U, u_i \cdot u_j = 0, \forall j \neq i, \tag{2.8}$$

Here, $u_j \in \{0,1\}$ represents a binary variable indicating the association with 1 indicating association and 0 indicating the unassociated cell. For the access links of the UEs, we obtain

$$u_j = \begin{cases} 1 & \text{if } P_i G_{z,x} h_{z,x} T_{z,x} L_{(1m)} L_{\mathrm{z,x}}(\|\mathbf{z}-\mathbf{x}\|)^{-1} \\ & \qquad \geq P_j T_j G_j h_{z,y} T_{z,y} L_{(1m)} L_{\mathrm{z,y}}(\|\mathbf{z}-\mathbf{y}\|)^{-1}, \\ & \qquad \forall\, \mathbf{y} \in \phi_j, j \in \{\mathrm{m},\mathrm{s}\} | \mathbf{x} \in \phi_i, \\ 0, & \text{otherwise.} \end{cases} \tag{2.9}$$

Because the IAB nodes have large antenna arrays and can perfectly beam align towards the needed direction, the antenna gain over the links can be assumed to be the same, and backhaul link association can be determined using the minimum path loss rule.

$$x_{b,m} = \begin{cases} 1 & \text{if } L_{\mathrm{b_m}}(\|\mathbf{z}-\mathbf{x}\|)^{-1} \geq L_{\mathrm{b_m}}(\|\mathbf{z}-\mathbf{y}\|)^{-1}, \\ & \qquad \forall\, \mathbf{y} \in \phi_{\mathrm{m}} | \mathbf{x} \in \phi_{\mathrm{m}}, \\ 0, & \text{otherwise.} \end{cases} \tag{2.10}$$

On the other hand, for resource allocation, the mmWave bandwidth available is shared in to the access and backhaul links such that

$$\begin{cases} B_{\text{Backhaul}} = \mu B, \\ B_{\text{Access}} = (1-\mu) B. \end{cases} \tag{2.11}$$

Here, $\mu \in [0,1]$ represents the percentage of bandwidth resources on backhaul links. Moreover, B_{backhaul} and B_{access} represent the backhaul and access bandwidths, respectively, while B is the total bandwidth. The bandwidth share for each SBS by the fiber backhauled MBS is proportional to its instantaneous load. Here, each SBS informs its current load to its associated MBS. The backhaul-related bandwidth for the j-th node is then given by

$$B_{\text{backhaul},j} = \frac{\mu B N}{\sum\limits_{\forall\, j} N_j} . \forall j, \tag{2.12}$$

Here N_j is the number of UEs connected at the jth BS and the access bandwidth is equally shared among the connected UEs according to a round robin schedule.

$$B_{\text{access,u}} = \frac{(1-\mu) B}{\sum\limits_{\forall\, u} N_{j,u}}, \tag{2.13}$$

where N represents the number of UEs at the considered SBS and j denotes each SBS associated to the MBS. Moreover, u denotes the UEs. $N_{j,u}$ is the load at the j^{th} node of which the u is associated. The signal-to-interference-plus-noise ratio (SINR) values obtained are given by

$$\text{SINR} = P_{\mathrm{r}} / (I_{\mathrm{u}} + N_0). \tag{2.14}$$

Here, N_0 represents the noise power. Then, the rates experienced by the UEs in access link is given by

$$R_\mathrm{u} = \begin{cases} \frac{(1-\mu)B}{N_m} \log(1 + \mathrm{SINR}(x_\mathrm{u})), \quad \text{if } \mathbf{x}_\mathrm{c} \in \phi_\mathrm{m}, \\ \min\Bigg(\frac{(1-\mu)BN}{\sum\limits_{\forall u} N_{j,u}} \log(1 + \mathrm{SINR}(x_\mathrm{u})), \\ \frac{\mu BN}{\sum\limits_{\forall j} N_j} \log(1 + \mathrm{SINR}(x_\mathrm{b})) \Bigg), \text{if } \mathbf{x}_c \in \phi_\mathrm{s} \end{cases} \tag{2.15}$$

$$R_\mathrm{b} = \frac{\mu BN}{\sum\limits_{\forall j} N_j} \log(1 + \mathrm{SINR}(x_\mathrm{b})), \tag{2.16}$$

where m is the associated MBS and s is the SBS. Depending on the association cell, there are two data rate scenario in the access links. The case in which UEs are associated to MBSs, as denoted by $x_\mathrm{c} \in \phi_\mathrm{m}$ in (2.15) is the first. Since the MBSs are fiber-connected, the rate will depend on the access bandwidth available at the UE. Secondly, the case in which UEs are connected to SBSs, as denoted by $x_\mathrm{c} \in \phi_\mathrm{s}$ in (2.15). Here the SBSs have the shared backhaul bandwidth constraint from the MBS donor, and thus UE data rates is the minimum between backhaul and access data rate. Figure. 2.3 illustrates the dynamic resource allocation strategy in the IAB deployment.

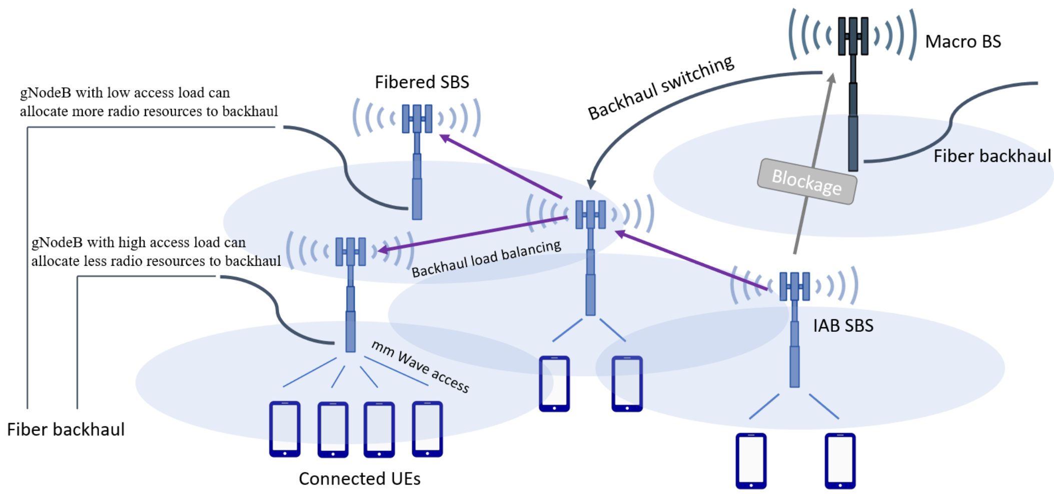

Figure 2.3: Dynamic resource allocation and topology adjustments for better efficient network.

2.5 Hybrid IAB network with fiber backhauled SBSs

Now, we make the network hybrid by providing fiber access to some of the small BSs in the previously discussed IAB network. Thus in contrast with the pure IAB network that we described earlier, this new deployment will comprise of both wirelessly backhauled SBSs as well as fiber backhauled SBSs. We select which SBSs to fiber connect randomly without using location based optimization. The MBSs have no difference from the previously discussed IAB network and will continue to have fiber access. This is also defined as a two tier multi cell frame work which gives us the flexibility to understand the performance of the pure IAB network in comparison. The data rates of the UEs connected to MBSs will follow the same relationship described in (2.15). However, now since some of the UEs will connect to fiber backhauled SBSs the UEs will experience three types of rates of which the MBS connected UEs will have rates same as earlier in accordance with (2.15). The wirelesslly backhauled SBS connected UEs will also experience data rates in accordance with (2.15) while the data rates of the fibered SBS connected UEs can then be expressed as,

$$R_u = \frac{B}{N_\mathrm{s}} \log(1 + SINR(x_\mathrm{u})), \text{if } \mathbf{x}_\mathrm{c} \in \phi_\mathrm{s} \tag{2.17}$$

The network will therefore have three forms of connections and the individual UE rates will behave according to the form the person's connection has been established.

3

Simulation Results

In this Chapter, we present and discuss the interesting results from the simulations. After describing our setup and presenting the main behaviour of IAB network in terms of network density and bandwidth allocation, we describe the results in three sections. In Chapter 3.1 we discuss the effect of rain, blocking and tree foliage on IAB network followed by the discussion which compares fiber backhauled network with IAB in Chapter 3.2. Here, we discuss based on performance as well as the cost. Next, in Chapter 3.3 we present the results and discuss the IAB network in 3D use case where we implement the network described in Chapter 2.1.2.
The system parameters are as of Table 3.1 unless otherwise explicitly stated.

Table 3.1: Simulation parameters

Parameters	Value
Carrier frequency	28 GHz
Minimum data rate threshold	100 Mbps
Bandwidth	1 GHz
BS and UE density	{MBS, SBS, UE} = (8, 100, 500) /km^2
Blocking	{Density, Length} = (500 /km^2, 5m)
Path loss exponents	{LoS, NLoS} = (2, 3)
Main lobe antenna gains	{MBS, SBS, UE} = (24, 24, 0) dBi
Side lobe antenna gains	{MBS, SBS, UE} = (-2, -2, 0) dBi
Bias factors	(1,1)
Noise power	5 dB
In-leaf percentage	20%
Tree depth	5 m
Blocking length	5 m
Antenna heights	{MBS, SBS, UE} = (25,10,1) m

The network is deployed in a disk of radius of D=1 km where rain occurrence, vegetation distributions are also probable according to ITU models described previously. In our analysis, we also deploy the IAB setup in both urban and rural areas, to get better insights and comparisons. Our metric of interest is the service coverage probability defined as the fraction of the UEs which have instantaneous UE data rates higher than or equal to a threshold R_{th}. That is, using (2.15), the service coverage probability is given by

$$\rho = \Pr(R_{\text{U}} \geq R_{\text{th}}). \tag{3.1}$$

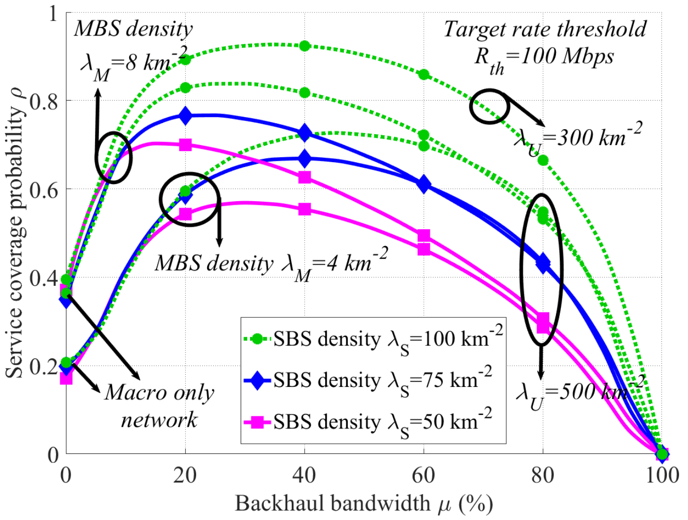

Figure 3.1: Service coverage probability as a function of backhaul bandwidth allocation percentage μ for a dense network, blocking density $\lambda_\mathrm{B} = 500\ \mathrm{km}^{-2}$ and $P_\mathrm{MBS}, P_\mathrm{SBS}, P_\mathrm{UE} = (40, 24, 0)$ dBm and no rain (See Table 3.1 for more parameters).

Service coverage probability is obtained as the fraction of UEs which have instantaneous UE data rates higher than the R_th.

In Figure. 3.1, we observe the results of the service coverage probability as a function of backhaul bandwidth allocation percentage μ considering the SBS density λ_S=50, 75 and 100 per km^2. As we see, depending on the network density there is an optimum μ in terms of the performance metric ρ. The optimum value tends to increase with the increase of SBS density. This is due to the increased backhaul resource requirement for the rising number of BSs. The maximum service coverage probability also increases with the increasing network density. IAB-type SBSs in the two tier network leads to considerable performance improvement, compared to the MBS only network. For instance, with the parameter settings of Figure. 3.1, the coverage probability increases from 0.36 in the cases with only MBSs of $\lambda_\mathrm{M} = 8$ per km^2 to 0.83 in the cases with SBSs distributed by density $\lambda_\mathrm{S} = 75\ \mathrm{km}^2$.

Next we study the impact of blockage distribution, rain and tree foliage on the network's service coverage probability.

3.1 Effect of Rain, Blocking and Tree Foliage

In this section, we observe the service coverage probability with respect to surrounding infrastructure and external environmental factors. We present the results for both urban and rural areas. For rural areas we assume no blocking is present. Figure 3.2 describes the network's performance in the presence of rain while in Figures 3.3-3.4 we observe the effect of blocking on the IAB setup. At last, in Figure. 3.5 we observe the network's resilience in the presence of vegetation and trees.

In Figure 3.2 for the rain analysis, dense networks with λ_S=50, 75 and 100 km^{-2} are

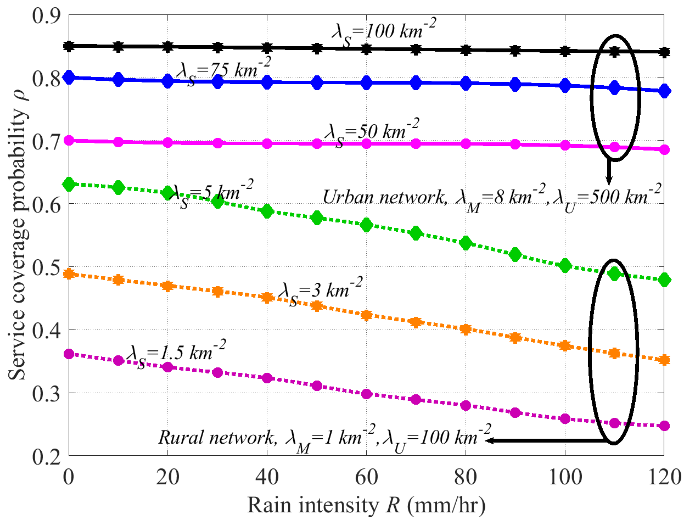

Figure 3.2: Service coverage probability of IAB network as a function of rain intensity for dense and rural network, with R_{th} = 100 Mbps, λ_{B}= 500 km^{-2} and $P_{\text{MBS}}, P_{\text{SBS}}, P_{\text{UE}} = (40, 24, 0)$ dBm for urban area and R_{th} = 50 Mbps, $P_{\text{MBS}}, P_{\text{SBS}}, P_{\text{UE}} = (45, 33, 0)$ and no blocking for rural area (See Table 3.1 for more parameters).

used to study the effects in urban areas while in rural areas we use λ_{S}=1.5, 3 and 5 km^{-2}. The minimum UE access data rate R_{th} for the evaluation is 100 Mbps and the blocking density λ_{B} is 500 km^{-2} to align with the urban areas' conditions while it is 50 Mbps and no blocking in rural areas. To facilitate long hop transmissions, the power of the SBSs and MBSs in rural network are increased to 33 dBm and 45 dBm respectively while the λ_{U} is 100 km^{-2} to represent the lower access connections in those areas. It should be noted that rains greater than 30 mm/hr are extremely high and the occurrences are rare. As we observe in the urban areas, the coverage probabilities exhibit drastically high resilience towards the rain conditions modeled by ITU-R. This is due to the smaller link distances found in urban areas. In rural conditions, the network is still resilient for rainfall upto 30 mm/hr. However, in contrast to the dense network we previously discussed, the considerable drop in performance is due to the increased hop lengths in rural or suburban conditions.

In Figures. 3.3-3.4, we observe the dense networks in urban areas for the effect of blocking. As we observe, the service coverage probability of IAB networks in urban areas are resilient for blocking. Increasing the blocking densities to much higher numbers reduces the performance. However, more denser the network becomes with SBSs it shows more resilience towards the blocking. This is facilitated as the UEs continued to associate to the readily available nearest SBS with higher probability of LoS than in a sparse node distribution. As we observe, the IAB network is more sensitive for blocking density increase than the rain when the network is dense. This is evident due to the LoS and NLoS characteristic behaviour of mmWaves.

In Figure. 3.5 we observe the above described IAB network in rural areas for the

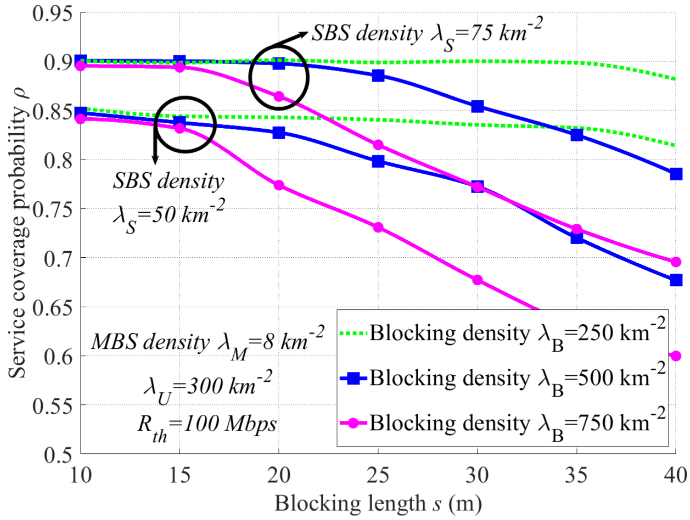

Figure 3.3: Service coverage probability of IAB network as a function of blocking length with $P_{\mathrm{MBS}}, P_{\mathrm{SBS}}, P_{\mathrm{UE}} = (40, 24, 0)$ dBm for dense network (See Table 3.1 for more parameters).

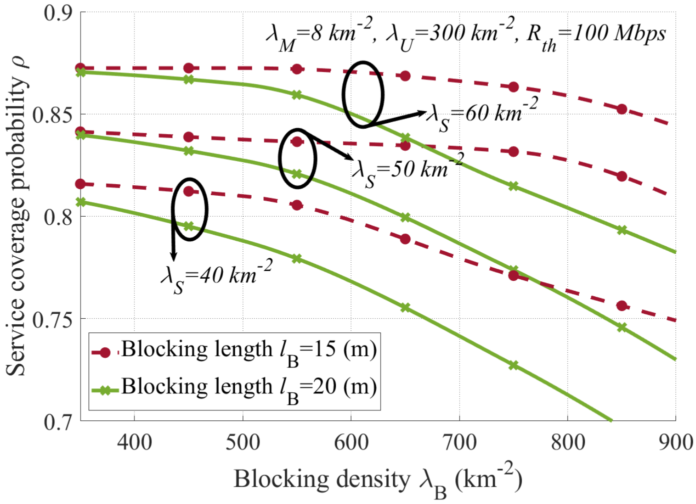

Figure 3.4: Service coverage probability of a dense IAB network as a function of blocking density λ_{B}, with $P_{\mathrm{MBS}}, P_{\mathrm{SBS}}, P_{\mathrm{UE}} = (40, 24, 0)$ dBm, and no rain/tree foliage (See Table 3.1 for more parameters).

effects of tree foliage. Well known FITU model described in Chapter 2.3 is used keeping the in-leaf percentage for 20% of the vegetation. It depicts that the tree foliage has some considerable effect on the rural network after a l_{T} value specific to the network depending on the number of IAB nodes and tree line density. This value is proportional to the SBS density while is inversely proportional to the λ_{T}. An exponential decay of service coverage probability follows after this resilient point described earlier. For a network with $\lambda_{\mathrm{S}} = 5$ km^{-2} and $\lambda_{\mathrm{T}} = 250$ km^{-2}, this point lies around 10 m of tree line length while it reduces close to 5 m in the case of $\lambda_{\mathrm{S}} = 3$ km^{-2} and $\lambda_{\mathrm{T}} = 750$ km^{-2}. Thus, in the presence of tree foliage, more IAB

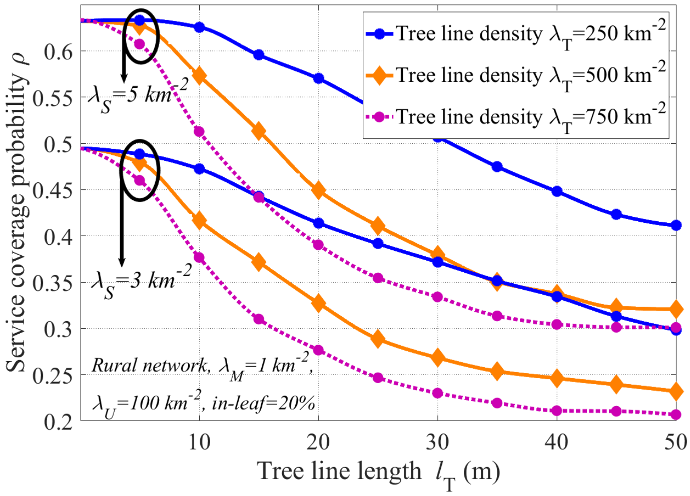

Figure 3.5: Service coverage probability of the rural IAB network in the presence of vegetation as a function of tree line length l_T with $R_{th} = 50$ Mbps and $P_{MBS}, P_{SBS}, P_{UE} = (45, 33, 0)$ dBm, d=5m, no rain and blocking (See Table 3.1 for more parameters).

nodes are required to achieve the same performance level. However, it is seen that for low to moderate tree foliage levels, IAB network continues to perform well even in rural areas with less SBS density or larger hop lengths.

In Figure. 3.6 we investigate the effect of antenna gain on the IAB network in terms of service coverage probability. The side lobe gain is -2 dBm in all cases, while transmit power of MBSs and UEs are 40 dBm and 0 dBm respectively. The service coverage probability ρ approximates into a logarithmic behavior and tends to become gradually constant after passing a specific antenna gain point depending on the SBS density and SBS transmit power. After the linear region, the network with $\lambda_S = 100$ km^{-2} and transmit power P_{SBS}=24 dBm closely fits with the network, $\lambda_{SBS} = 50$ km^{-2} and P_{SBS}=28 dBm. Thus in a trade off with the Opex power costs and green efficiency of the network, the number of IAB nodes could be reduced which in turn reduces the Capex costs involved in the network.

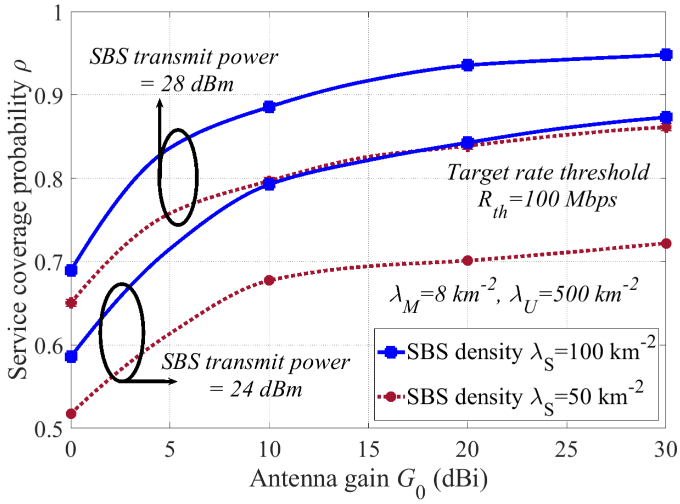

Figure 3.6: Service coverage probability as a function of main lobe antenna gain G_0 for a dense network without rain with $\lambda_B = 500$ km^{-2} and $P_{\mathrm{MBS}}, P_{\mathrm{UE}} = (40, 0)$ dBm (See Table 3.1 for more parameters).

3.2 Fiber backhauled network and IAB network

In this section we present and compare the results for IAB setup with a network comprising with fiber backhauled SBSs. Moreover the hybrid IAB setup described in Chapter 2.5, is also used for the evaluation. Figures. 3.7-3.9 demonstrate the results as functions of different network density parameters.

3.2.1 Performance perspective

Figure. 3.7 plots the service coverage probability as a function of the percentage of fiber backhauled SBSs in the previously discussed all IAB network considering $\lambda_S = 50$ and 100 km^{-2}. Refer to Chapter 2.5 to see how we implement the setup. We observe the behaviour for both R_{th}=100 Mbps and 80 Mbps. As we see, with the increase of fiber backhauled SBSs, the service coverage probability of the pure IAB network can be fine optimized to give better performance. This is due to the availability of more radio resources at some percentage of the IAB network to serve the needs. The increase is approximately linear in the considered region. In our study we select the nodes to fiber-connect randomly. However, if location based identification is carried out on selecting the most suitable SBSs to fiber-connect, the performance can be further improved.

In Figure. 3.8 we plot the service coverage probability with respect to SBS densities of pure IAB, hybrid IAB and all fiber backhauled networks. As we see, the performances vary as, Macro only network<all IAB network<Hybrid network with 30% SBSs fiber-connected<All fibered network. As a second scenario using the information from Figure. 3.8, in Figure. 3.9 we depict how much equivalence of IAB nodes are needed to achieve the same performance as of a fiber backhauled network.

As we observe for a wide range of parameter settings, the same performance as in the

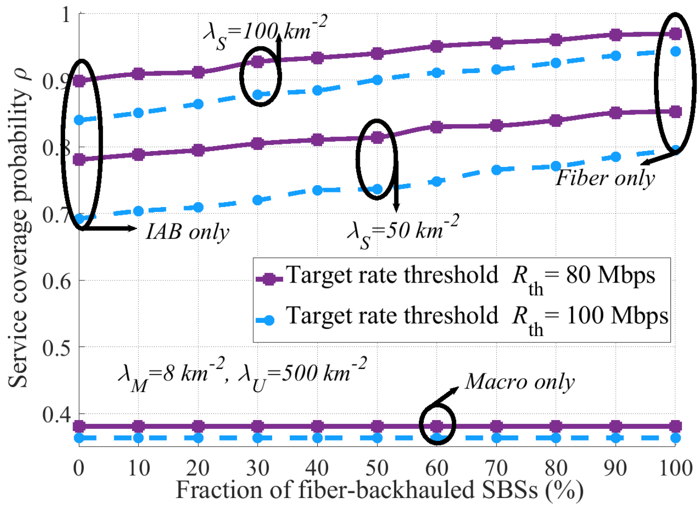

Figure 3.7: Service coverage probability as a function of fiber backhauled SBS percentage for a dense network with λ_B= 500 km^{-2}, no rain and P_{MBS}, P_{SBS}, P_{UE} = $(40, 24, 0)$ dBm (See Table 3.1 for more parameters).

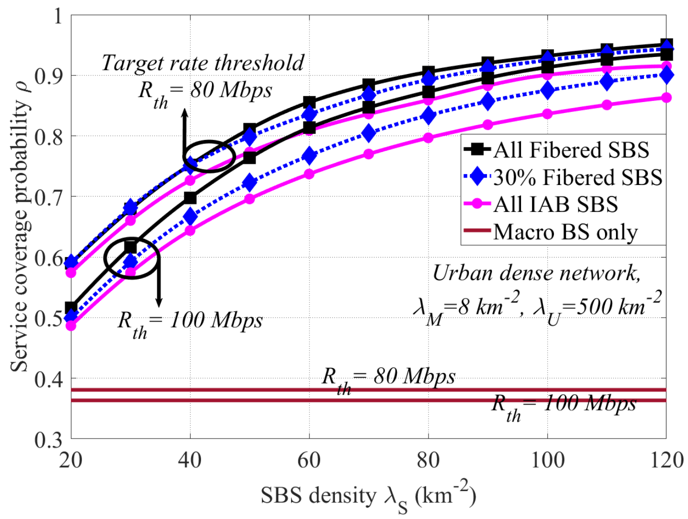

Figure 3.8: Dense IAB network without rain in comparison with fiber backhauled network for service coverage probability as a function of SBS density with λ_B = 500 km^{-2} and P_{MBS}, P_{SBS}, P_{UE} = $(40, 24, 0)$ dBm (See Table 3.1 for more parameters).

fully fiber-connected networks can be achieved by the IAB network, with relatively small increment in the number of IAB nodes. As we see, a fiber-connected network with SBSs densities 60 km^{-2} corresponds to a service coverage probability of 0.76 which is the same in case of IAB network having a density of λ_S = 85 km^{-2}. Another interesting fact is that, with 30% of the SBSs fiber backhauled, which is a feasible deployment condition, the required increment further narrows.

Interestingly, with a 30% of SBSs having fiber connections, which is practically reasonable, the needed increment further narrows.

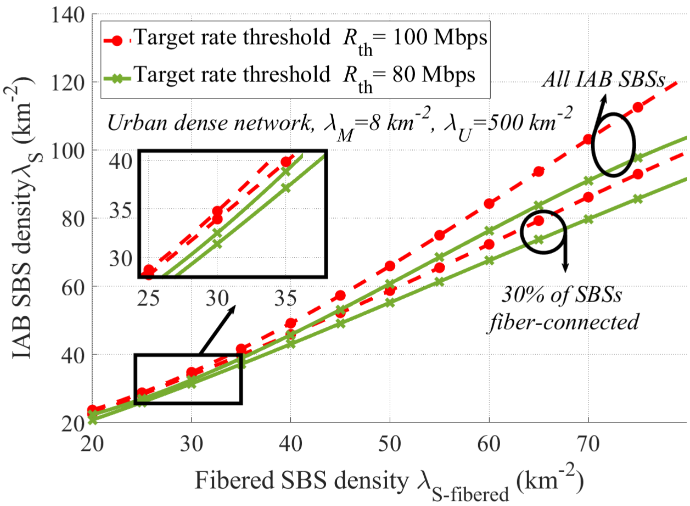

Figure 3.9: Density of IAB nodes sufficing the performance of fiber backhauled network with $\lambda_B = 500$ km^{-2}, no rain for $P_{MBS}, P_{SBS}, P_{UE} = (40, 24, 0)$ dBm (See Table 3.1 for more parameters).

3.2.2 Cost perspective

We observe that fiber backhauled networks out-perform the IAB networks in terms of service coverage probability. However from Figure. 3.9 we also observe that the number IAB nodes needed to reach the all fiber network performance is not significantly high. Regardless of the fact that capex for fiber vastly varies in different regions due to many factors including labour cost, fiber laying accounts to a significant fraction of the total network operator costs. According to [36] the costs are in the range of 20000 GBP/km while [37, 38] estimates the to cost to be 100000-200000 USD/km in metropolitan areas, with a large portion 85% of the total figure tied to trenching and installation.
However in contrast, IAB networks do not involve digging and fiber laying capex costs. Although, the node cost for IAB networks is higher than that of an all fiber network, the difference is competitive with the fiber laying costs. According to [39] the equipment capex for network densification through small BSs in 5G is 2500 GBP per unit. Moreover, IAB has crucial applicability in areas where digging is not permitted but rapid 5G deployments are needed. These cases include archaeological sites, difficult terrain conditions and various external factors.

3.3 IAB Network in 3D Use Case

In this section we study the service coverage probability in a 3D setup described in Chapter 2.1.2. Here, the blockages (as well as the distance between the nodes) are determined based on the geo information, i.e., the real world blocking terrain is considered using OpenStreetMap 3D environment. The results have been tested on a disk of radius $D = 0.5$ km spanning over the area surrounding and in close to Chalmers University of Technology, Gothenburg, Sweden.

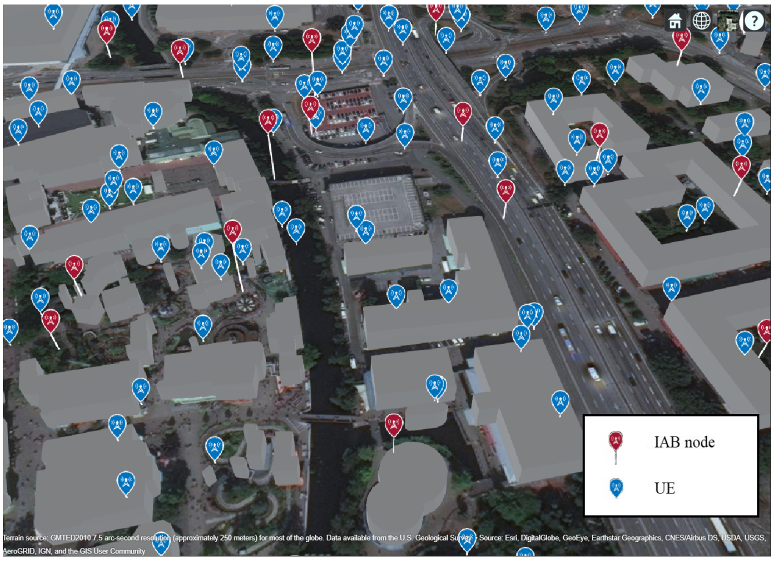

Figure 3.10: Distribution of the IAB network in 3D space with OpenStreetMap.

Figure 3.11: Example network realization of the 3D model

The steps followed in setting the things up are as below,

- Firstly, we use the same FHPPPs of SBSs, MBSs and UEs as of the 2D setup which are all spatially distributed in a disk of radius D. D in here is 0.5 km.
- In the above explained disk, we calculate all relative locations of MBSs, SBSs and UEs. ie., relative locations based on distances between each antenna instead of an absolute position.
- Now we give heights to the antennas depending on whether its a MBS, SBS or an UE using RF propogation tool box of Matlab.
- Next we choose a suitable absolute longitude latitude co-ordinate location to place our previously described distribution of antennas.
- Now we position the center of disk on absolute latitude, longitude location.

And then with the use of pre-calculated relative location data, we position the antennas on top of Google data obtained via OpenStreet3D map (which comes in an .osm file, and is imported to Matlab). This has height profiles of all blockings and physical obstacles. All of these antennas now has a height and also the blockings are 3D.

- Now from the antennas of SBSs and MBSs we construct links to the UEs, If it obstructs a building in the 3D space, then it is considered NLoS and otherwise is LoS.
- These LoS/NLoS link state matrix is then fed to the system setup described in Chapter 2.

Figures. 3.10-3.11 reveals the 3D spatial distribution of the network and its deployment. As shown, the elevation and topographical information of the buildings and blocking are used in determining the LoS conditions to estimate the received power levels at the IAB nodes.

Additionally, the Figures. 3.12-3.13 depict the service coverage probability of the IAB network on google model with terrain and building topography information. It should be noted that, the behaviour also changes in different cities depending on the amount of blocking while maintaining the characteristic shapes of the curves.

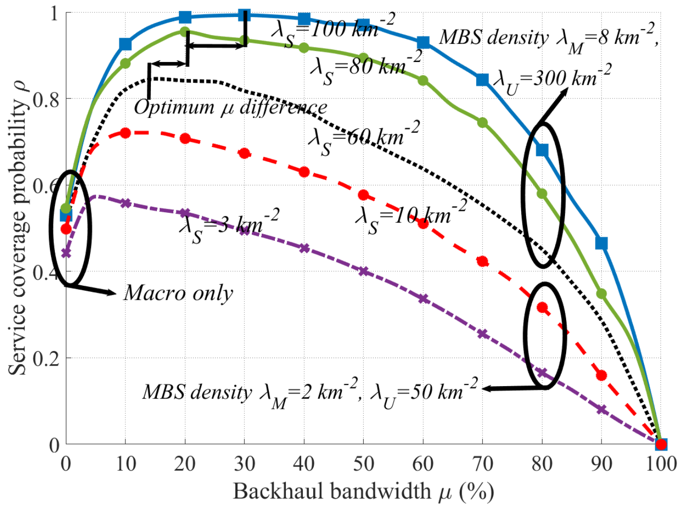

Figure 3.12: Service coverage probability as a function of backhaul bandwidth allocation percentage μ for dense network with $\lambda_{\mathrm{B}} = 500\ \mathrm{km}^{-2}$, $R = 0$ mm/hr, $R_{\mathrm{th}} = 100$ Mbps and $P_{\mathrm{MBS}}, P_{\mathrm{SBS}}, P_{\mathrm{UE}} = (40, 24, 0)$ dBm for the 3D use case (See Table 3.1 for more parameters).

In Figure. 3.12 we plot the service coverage probability as a function of backhaul bandwidth partitioning percentage μ for the IAB network in 3D plane, which shows similar characteristical behaviour with reference to the Figure. 3.1 of 2D plane. This demonstrates that the behaviour in 3D blocking use case is also quite close with the stochastic geometric model we used earlier with the germ grain blocking model.

Thus we can predict that the germ-grain blocking model gives reasonable prediction on the blindspot probability. Also the optimum μ keeps increasing with the SBS density. The optimum μ which maximizes the service coverage probability is around

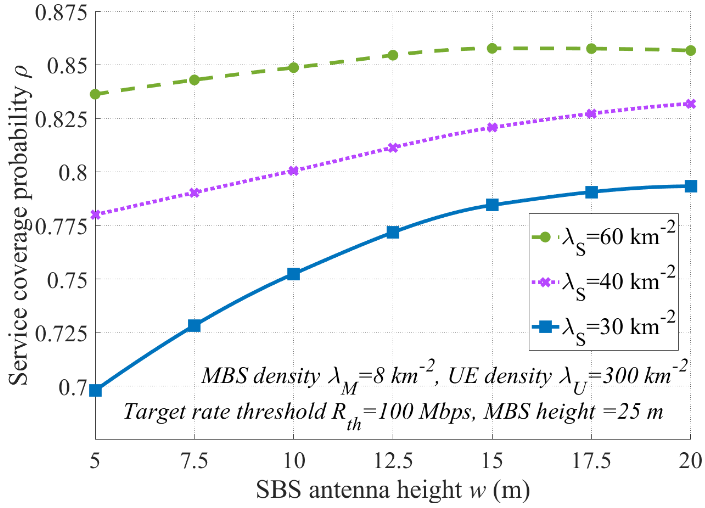

Figure 3.13: Service coverage probability as a function SBS antenna height w for a dense network with $P_{\mathrm{MBS}}, P_{\mathrm{SBS}}, P_{\mathrm{UE}} = (40, 24, 0)$ dBm for the 3D use case (See Table 3.1 for more parameters).

15% in the network with $\lambda_{\mathrm{S}} = 60$ km^{-2} while it is close to 30% in the network with $\lambda_{\mathrm{S}} = 100$ km^{-2}

In Figure. 3.13 we compare the service coverage probability of the IAB network with respect to antenna heights of SBSs. We see that increasing the height of the SBSs helps to reduce the required number of IAB nodes notably. For instance, parameter settings of Figure. 3.13 depicts that the same coverage probability as in the cases with density $\lambda_{\mathrm{S}} = 40$ km^{-2} and height $w = 5$ m is achieved by a setup having $\lambda_{\mathrm{S}} = 30$ km^{-2} and $w = 15$ m. The increase of antenna heights give logarithmic increase to its performance, while the gradient decreases with the network density. This is due to the fact that, more denser the network is, it gets higher probability to find out LoS link which eventually shows lesser impact by the increase of antenna height than the ones with lower densities.

4
Conclusions

A stochastic geometry model based multi cellular multi tier HetNet framework was established to model mmWave networks for IAB. With the use of well known models characterizing the mmWave behaviour, we investigated the performance of IAB networks in terms of service coverage probability. Dynamic resource allocation strategies were used for flexible deployment. We also evaluated the the network's resilience over the external environmental factors including rain, vegetation and blocking. A hybrid IAB network of which some small base stations are fiber backhauled was then compared against a pure IAB scenario. Later, a relative cost description of the IAB with other backhauling options was done which helped to give insight on where and which extent the IAB suits. Finally, the IAB network was deployed on top of OpenStreetMap topography data to observe the network performance in 3D plane in which we observed the effects of antenna heights on service coverage probability.

Our analysis revealed that there is an optimum IAB node density satisfying the same performance as of a pure fiber backhualed network. The performance of IAB network was well above the macro-only network and is lesser than an all fiber backhauled network. However by increasing the IAB network density or fiber backhauling some percentage of the nodes resulted the network to reach fiber backhaul performance. In the 3D use case, we observed that by increasing the antenna heights of the network the performance of more dense network could be reached. However the results were not notably improved in dense networks, due to the availability of nearby node with high probability of LOS even at street level. Also we observed that the curves were characteristically close to that of 2D use case which used germ-grain stochastic blocking model. This indicated that the germ-grain model we used approximated the blind spot probability for the links with notable precision. The network was resilient for rain under normal condions in terms of coverage probability and ergodic downlink data rates. The dense networks in urban areas showed a significant resilience towards blocking which indicates the suitability of IAB in urban areas. IAB in rural areas too were resilient for minor and medium range of tree foliage presence. The resistance to foliage could be increased with network density.
As we demonstrated, IAB is a cost-effective replacement of fiber optics in dense metropolitan areas while the blockage and the rain are not problematic and also for the rural areas with lesser or modest vegetation presence.

5
Future Work

The thesis is contributing in identifying, understanding and designing of IAB network for 5G NR and beyond, focusing on a two tier multi cellular framework. The work also contributes on evaluating the performance of IAB network in different perspectives and multiple use cases described previously. Also, an article which includes the results of the thesis is drafted and is to be submitted to the IEEE Open Journal of the Communications Society (IEEE OJCOMS). The article focuses on IAB in different perspectives including IAB 3GPP discussions on Release 16, 17 and robustness analysis [40].
However, been a new and broad topic, there can be many improvements and research ideas that could be developed in future. They include,

- Identifying and optimizing the node locations that could be critical to have fiber connections in the IAB network using machine learning.
- Identify efficient algorithms for resource allocation.
- Conduct theoretical analysis of finite homogeneous poisson point process (FH-PPP) in IAB node distributions.
- Design of multi-hop IAB networks.
- Study on better interference cancellation in the in-band IAB.
- Deriving the optimal value for access and backhaul bandwidth allocation.

Bibliography

[1] Ericsson, “Mobile data traffic growth outlook” https://www.ericsson.com/en/mobility-report/reports/november-2018/mobile-data-traffic-growth-outlook

[2] H. Dahrouj, A. Douik, F. Rayal, T. Y. Al-Naffouri and M. Alouini, "Cost-effective hybrid RF/FSO backhaul solution for next generation wireless systems," IEEE Trans. Wireless Commun, vol. 22, no. 5, pp. 98-104, Oct. 2015.

[3] X. Artiga, J. Nunez-Martinez, A. Perez-Neira, G. J. L. Vela, J. M. F. Garcia and G. Ziaragkas, "Terrestrial-satellite integration in dynamic 5G backhaul networks," 8th Advanced Satellite Multimedia Systems Conference and the 14th Signal Processing for Space Communications Workshop (ASMS/SPSC), Palma de Mallorca, Sep. 2016, pp. 1-6, doi: 10.1109/ASMS-SPSC.2016.7601470

[4] S. Julião et al., "High performance microwave point-to-point link for 5G backhaul with flexible spectrum aggregation," 2015 IEEE MTT-S International Microwave Symposium, Phoenix, AZ, May 2015, pp. 1-4, doi: 10.1109/MWSYM.2015.7166817.

[5] S. Z. Du, K. Aronkytö, J. Putkonen, J. Kapanen, E. Ohlmer and D. Swist, "5G E-band backhaul system evaluations: Focus on moving objects and outdoor to indoor transmission," 2017 European Conference on Networks and Communications (EuCNC), Oulu, June 2017, pp. 1-5, doi: 10.1109/EuCNC.2017.7980764.

[6] B. Makki, T. Svensson, T. Eriksson and M. Alouini, "On the Performance of RF-FSO Links With and Without Hybrid ARQ," in IEEE Transactions on Wireless Communications, vol. 15, no. 7, pp. 4928-4943, July 2016.

[7] O. Tipmongkolsilp, S. Zaghloul, and A. Jukan, “The Evolution of Cellular Backhaul Technologies: Current Issues and Future Trends,” IEEE Commun. Surveys Tutorials, vol. 13, no. 1, 1st qtr. 2011, pp. 97–113.

[8] C. Dehos, J. L. González, A. D. Domenico, D. Kténas and L. Dussopt, "Millimeter-wave access and backhauling: the solution to the exponential data traffic increase in 5G mobile communications systems," IEEE Commun. Mag., vol. 52, no. 9, pp. 88-95, Sept. 2014.

[9] Y. Li, E. Pateromichelakis, N. Vucic, J. Luo, W. Xu and G. Caire, "Radio Resource Management Considerations for 5G Millimeter Wave Backhaul and Access Networks," IEEE Commun. Mag., vol. 55, no. 6, pp. 86-92, June 2017

[10] 3GPP, “Overview of 3GPP Release 10 V0.2.1 (2014-06)", Available at: https://www.3gpp.org/ftp/Information/WORK_PLAN/Description_Releases/

[11] O. Teyeb, A. Muhammad, G. Mildh, E. Dahlman, F. Barac and B. Makki, "Integrated Access Backhauled Networks," in Proc. IEEE VTC-Fall'2019, Honolulu, HI, USA, Sept. 2019, pp. 1-5.

[12] M. N. Islam, S. Subramanian and A. Sampath, "Integrated Access Backhaul in Millimeter Wave Networks," in Proc. IEEE WCNC'2017, CA, USA, Mar. 2017, pp. 1-6.

[13] M. N. Islam, N. Abedini, G. Hampel, S. Subramanian and J. Li, "Investigation of performance in integrated access and backhaul networks," in Proc. IEEE INFOCOM'2018, HI, USA, Apr. 2018, pp. 597-602.

[14] Y. Li, J. Luo, R. A. Stirling-Gallacher, G. Caire, "Integrated Access and Backhaul Optimization for Millimeter Wave Heterogeneous Networks," arXiv:1901.04959, Available at: https://arxiv.org/abs/1901.04959.

[15] Y. Liu, A. Tang and X. Wang, "Joint Incentive and Resource Allocation Design for User Provided Network under 5G Integrated Access and Backhaul Networks," IEEE Trans. Net. Science and Engineering, in press, Apr. 2019.

[16] A. HasanzadeZonuzy, I-H. Hou, S. Shakkottai, "Broadcasting Real-Time Flows in Integrated Backhaul and Access 5G Networks," arXiv:1901.07728, Available at: https://arxiv.org/abs/1901.07728

[17] M. Polese, M. Giordani, A. Roy, D. Castor and M. Zorzi, "Distributed Path Selection Strategies for Integrated Access and Backhaul at mmWaves," in Proc. IEEE GLOBECOM'2018, Abu Dhabi, United Arab Emirates, Dec. 2018, pp. 1-7

[18] M. N. Kulkarni, A. Ghosh, J. G. Andrews, "Max-Min Rates in Self-backhauled Millimeter Wave Cellular Networks" arXiv:1805.01040, Available at: https://arxiv.org/abs/1805.01040

[19] M. Polese, M. Giordani, A. Roy, S. Goyal, D. Castor and M. Zorzi, "End-to-End Simulation of Integrated Access and Backhaul at mmWaves," in Proc. IEEE CAMAD, Sept. 2018, Barcelona, Spain, pp. 1-7.

[20] M. N. Kulkarni, J. G. Andrews and A. Ghosh, "Performance of Dynamic and Static TDD in Self-Backhauled Millimeter Wave Cellular Networks," IEEE Trans. Wireless Commun., vol. 16, no. 10, pp. 6460-6478, Oct. 2017.

[21] B. Makki, M. Hashemi, L. Bao and M. Coldrey, "On the Performance of FDD and TDD Systems in Different Data Traffics: Finite Block-Length Analysis," in Proc. IEEE VTC-Fall, Aug. 2018, IL, USA, Aug. 2018, pp. 1-5.

[22] C. Saha, M. Afshang and H. S. Dhillon, "Integrated mmWave Access and Backhaul in 5G: Bandwidth Partitioning and Downlink Analysis," in Proc. IEEE ICC'2018, MO, USA, May 2018, pp. 1-6

[23] S. Singh, M. N. Kulkarni, A. Ghosh and J. G. Andrews, "Tractable Model for Rate in Self-Backhauled Millimeter Wave Cellular Networks," IEEE J. Sel. Areas Commun., vol. 33, no. 10, pp. 2196-2211, Oct. 2015.

[24] C. Saha, H. S. Dhillon, "Millimeter Wave Integrated Access and Backhaul in 5G: Performance Analysis and Design Insights," arXiv:1902.06300, Available at: https://arxiv.org/pdf/1902.06300.pdf

[25] A. Fouda, A. S. Ibrahim, I. Guvenc and M. Ghosh, "UAV-Based In-Band Integrated Access and Backhaul for 5G Communications," in Proc. IEEE VTC-Fall'2018, IL, USA, Aug. 2018, pp. 1-5.

[26] N. Tafintsev, D. Moltchanov, M. Gerasimenko, M. Gapeyenko, J. Zhu, S. Yeh, N. Himayat, S. Andreev, Y. Koucheryavy and M. Valkama, "Aerial Access and Backhaul in mmWave B5G Systems: Performance Dynamics and Optimization," in IEEE Commun. Mag., vol. 58, no. 2, pp. 93-99, Feb. 2020.
[27] S. M. Azimi-Abarghouyi, B. Makki, M. Nasiri-Kenari and T. Svensson, "Stochastic Geometry Modeling and Analysis of Finite Millimeter Wave Wireless Networks," IEEE Trans. Veh. Technol. IEEE Trans. Veh. Commun.* (1955-1966), vol. 68, no. 2, pp. 1378-1393, Feb. 2019.
[28] E. Meesa-ard, S. Pattaramalai, MD. Madapatha, Outage Probability of Mobility Incorporated alpha-mu Fading Distribution with Co-channel Interference in Heterogeneous Networks. In2018 IEEE International Conference on Smart Internet of Things (SmartIoT) 2018 Aug 17 (pp. 76-80). IEEE.
[29] E. Meesa-ard, S. Pattaramalai, MD. Madapatha, Evaluating the Impact of Mobility over K-Il Generalized Fading Channels in Digital Communication. In2018 8th International Conference on Electronics Information and Emergency Communication (ICEIEC) 2018 Jun 15 (pp. 35-39). IEEE.
[30] B. Bartłomiej, "Notes on Random Geometric Models–Random Graphs, Point Processes and Stochastic Geometry." (2017), Available at:https://hal.inria.fr/cel-01654766/document
[31] T. S. Rappaport, Y. Xing, G. R. MacCartney, A. F. Molisch, E. Mellios and J. Zhang, "Overview of Millimeter Wave Communications for Fifth-Generation (5G) Wireless Networks—With a Focus on Propagation Models," IEEE Trans. Antennas Propag, vol. 65, no. 12, pp. 6213-6230, Dec. 2017.
[32] ITU-R Recommendation P.838-3: 'Specific attenuation model for rain for use in prediction methods', International Telecommunication Union, 2006.
[33] Diggle, J. Peter, "Some statistical aspects of spatial distribution models for plants and trees, College of Forestry, Swedish University of Agricultural Sciences," No. 162, 1982.
[34] M.A Abu-Rgheff, "5G Physical Layer Technologies",Wiley, 2019, pp. 303-313
[35] Khan, T. Ahmed, A. Alkhateeb, and R. W. Heath, "Millimeter wave energy harvesting."IEEE Trans. Wireless Commun.15, no. 9, pp. 6048-6062, 2016.
[36] Oughton, Edward J., and Zoraida Frias. "Exploring the cost, coverage and rollout implications of 5G in Britain." Cambridge: Centre for Risk Studies, Cambridge Judge Business School (2016).
[37] H. A. Willebrand and B. S. Ghuman, "Fiber optics without fiber," IEEE Spectrum, vol. 38, no. 8, pp. 40–45, Aug. 2001.
[38] GSMA, "Mobile Backhaul: An Overview." GSMA.com, https://www.gsma.com/futurenetworks/wiki/mobile-backhaul-an-overview/ (accessed May. 1, 2020).
[39] 5G NORMA. 2015. 'Deliverable D2.1: Use Cases, Scenarios and Requirements'. 5G PPP. http://www.it.uc3m.es/wnl/5gnorma/deliverables.html
[40] C. Madapatha, B. Makki, C. Fang, O. Teyeb, E. Dahlman, M.S. Alouni, T. Svensson, "On Integrated Access and Backhaul Networks: Current Status and Potentials", Submitted to IEEE Open Journal of the Communications Society (OJ-COMS), June 2020. arXiv preprint arXiv:2006.14216, Available at: https://arxiv.org/abs/2006.14216